DOI: 10.1002/ejic.200600445

Synthesis, Structure and Magnetism of Metal-Organic Framework Materials with Doubly Pillared Layers

Hong-Peng Jia,[a] Wei Li,[a] Zhan-Feng Ju,[a] and Jie Zhang*[a]

Keywords: Metal-organic frameworks / Pillared-layer structure / Iron(II) / Cobalt(II) / Hydrothermal synthesis / Magnetic properties / Carboxylates

Two novel coordination polymers with a 3D pillared-layer framework, $[M^{II}(Tdc)(4,4'\text{-Bpy})]_n$ [M = Fe (**1**), Co (**2**); Tdc = thiophene-2,5-dicarboxylate; 4,4′-Bpy = 4,4′-bipyridine), have been hydrothermally synthesised and structurally characterised. A simultaneous reduction of iron(III) to iron(II) occurs under hydrothermal conditions in the self-assembly process of complex **1**. The complexes are isostructural and, in each complex, the metal ions are linked by double μ_2-carboxylate bridges in a *syn-syn* mode, giving rise to dinuclear units that are connected to each other by chelating carboxylate groups from the Tdc ligands in an approximately perpendicular orientation to form 2D rectangle-grid layers. The adjacent layers are held together through 4,4′-Bpy molecules in a double-pillar support fashion to give a 3D network with three intersecting perpendicular channels. Variable-temperature magnetic susceptibility measurements revealed weak antiferromagnetic coupling interactions in both complexes and a field-induced magnetic transition can be observed in **2**.

Introduction

There has been continuous interest in the design and synthesis of metal-organic coordination polymers and supramolecular architectures due to their potential applications in the fields of magnetism, porous materials, catalysis and nonlinear optical activities or molecular recognition.[1–6] In the rational development of new strategies for the crystal engineering of coordination networks and supramolecular architectures, the pillared-layer assemblies have been shown to be precursors in an efficient route for the construction of porous frameworks with controllable channel sizes and chemical functionalities.[7–9] In particular, the pillared-layer networks based on coordination bonds are more attractive than those based on the hydrogen-bonded assemblies owing to their high structural and thermal stabilities.[10–13] Although the advantages of the pillared-layer assemblies are generally due to their suitability for manipulation of the pore structures by means of simple modifications to the pillar module, the search for new layer-building units is also quite necessary for systematic fine-tuning of structural and functional features. In this paper, we report two novel coordination polymers with a 3D porous pillared-layer framework, namely $[Fe^{II}(Tdc)(4,4'\text{-Bpy})]_n$ (**1**) and $[Co^{II}(Tdc)(4,4'\text{-Bpy})]_n$ (**2**). Thiophene-2,5-dicarboxylate (Tdc) ligands link the metal ions by bridging and chelating carboxylate groups to form a rare type of 2D rectangle-grid layer containing the dimetallic carboxylate subunits in a mutually perpendicular orientation. Each 4,4′-Bpy ligand as a rigid spacer is coordinated to the axial positions of the metal ions, connecting the $[M^{II}(Tdc)]_n$ layers into a 3D coordination framework with twofold interpenetration. An interesting aspect of the structure is that the 4,4′-Bpy ligands bind to the layers in a double-pillar support fashion (Scheme 1), which results in a molecular architecture with a higher thermal stability. In addition, the Tdc ligand displays both chelating and μ_2-bridging carboxylate coordination modes in the assemblies (Scheme 2) and this is the first

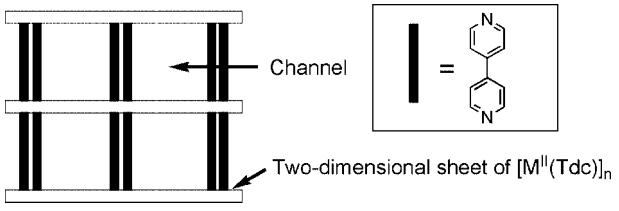

Scheme 1. Schematic representation of the doubly pillared-layer structures of $[M^{II}(Tdc)(4,4'\text{-Bpy})]_n$ (M = Fe, Co).

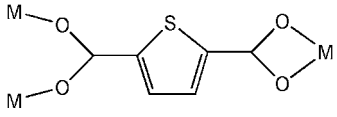

Scheme 2. Coordination mode of Tdc in complexes **1** and **2**.

[a] State Key Laboratory of Structural Chemistry, Fujian Institute of Research on the Structure of Matter, Chinese Academy of Sciences,
Fuzhou, Fujian 350002, China
Fax: +86-591-8371-0051
E-mail: zhangjie@fjirsm.ac.cn

Supporting information for this article is available on the WWW under http://www.eurjic.org or from the author.

observation of such behaviour for the Tdc ligand.[14] Variable-temperature magnetic susceptibility measurements revealed weak antiferromagnetic coupling interactions in both complexes and a field-induced magnetic transition can be observed in **2**.

Results and Discussion

Synthesis and Structural Description

Single-crystal X-ray diffraction analyses revealed that complexes **1** and **2** are isostructural and crystallise in the orthorhombic space group *Pccn*. As a representative example, the crystal structure of complex **1** is described here in detail. It is interesting to note that a simultaneous reduction of iron (III) to iron (II) occurs in the self-assembly process of complex **1** under hydrothermal conditions. There have been some reports that several metal ions can be reduced in the presence of 4,4′-Bpy under hydrothermal conditions. Although the mechanisms of redox reactions are still unknown, hydrothermal conditions are essential for achieving the reduced product.[15] The fundamental building unit of **1** is composed of a six-coordinate Fe^{II} centre, a Tdc ligand and a 4,4′-Bpy ligand. Each Fe^{II} centre exhibits a distorted octahedral geometry with two pyridyl nitrogen atoms (N1, N2D) from different 4,4′-Bpy ligands at the axial positions and four oxygen atoms in the equatorial plane of which two (O3A, O4B) are from two μ_2-bridging bidentate carboxylate groups from two different Tdc ligands and the other two (O1, O2) are from a chelating carboxylate group of a Tdc ligand, as shown in Figure 1. The Fe–O bond lengths are in the range of 1.999(3)–2.387(3) Å and the Fe–N bond lengths are 2.195(3) and 2.168(3) Å, respectively. The O1–Fe–O2 bite angle of 58.07(10)° is much smaller than the O3A–Fe–O4B bond angle of 117.90(12)°.

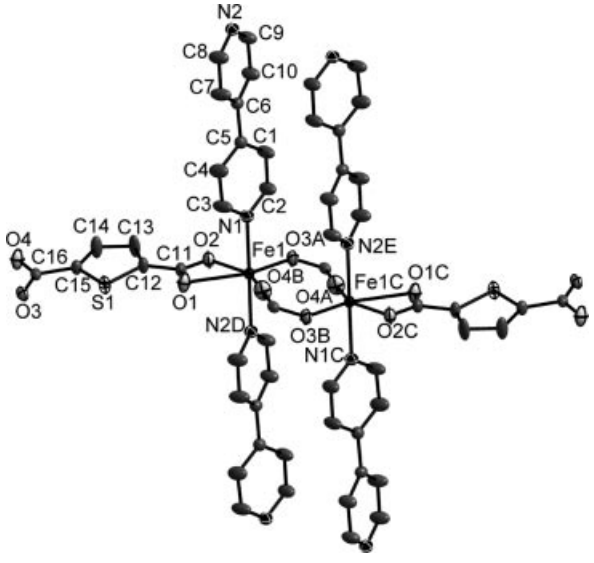

Figure 1. Coordination environment of the Fe^{II} ion with atom labelling in **1**. Hydrogen atoms are omitted for clarity.

Two equivalent Fe^{II} ions related by a twofold axis with a separation of 4.149 Å are bridged by two carboxylate groups from two different Tdc ligands in a *syn-syn* mode to form a dinuclear subunit. These dinuclear units are aligned approximately perpendicular to each other in the *ac* plane and linked further by additional Tdc ligands in a chelating mode to give rise to a neutral 2D sheet with a rectangular window of 8.8 × 11.0 Å (Figure 2). It is worthy of note that the orthogonal arrangement of dimetallic subunits within a 2D layer is still rare in metal carboxylate complexes in which dinuclear units are generally parallel to each other.[16] Each Tdc ligand coordinates to three Fe^{II} ions through the two terminal carboxylate groups in chelating and bridging modes, respectively, illustrating an unreported coordination mode for the Tdc molecule. An interesting aspect of the structure is that the 2D porous sheets are connected by 4,4′-Bpy ligands through the axial positions of both Fe^{II} centres in subunits to form a 3D doubly pillared-layer structure with three intersecting perpendicular channels (Figure 3). The whole structure can also be described as a 3D frame-

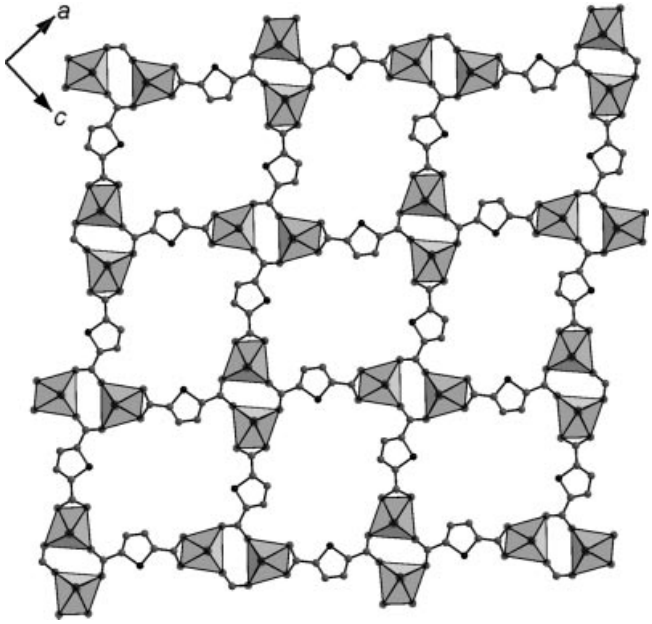

Figure 2. Perspective view of the $[Fe(Tdc)]_n$ sheet subunit with rectangular windows of about 8.8 Å × 11.0 Å. Hydrogen atoms are omitted for clarity.

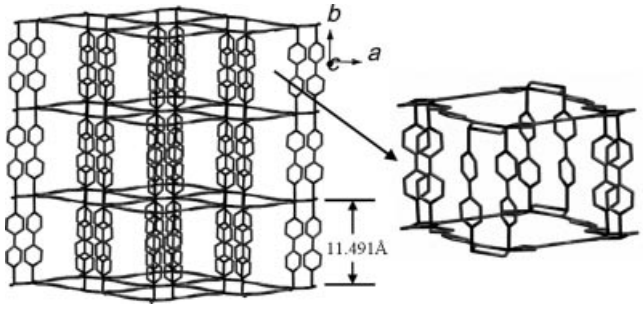

Figure 3. (a) Perspective view of the pillared-layer 3D network of **1**; (b) cuboid-like unit in **1**.

work composed of cuboid-like cavities with dimensions of 12.16 × 12.16 × 11.49 Å (based on the centre of the dinuclear subunit). The large cavities in the structure lead to a tendency to form an interpenetrating network. As shown in Figure 4, a twofold interpenetrating topological structure can be observed. The volume of the effective void is about 9.9% of the unit-cell volume in the self-inclusion structure.

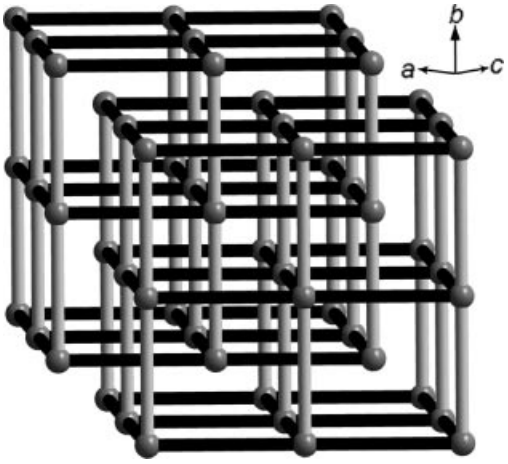

Figure 4. Structure topology of **1** displaying twofold interpenetration (darker and grey rods representing the Tdc and 4,4′-Bpy ligands, respectively).

Thermogravimetric Analysis

The thermal stabilities of the two complexes were determined by thermogravimetric analysis (TGA) in air with a heating rate of 20 °C min^{-1}. Complexes **1** and **2** exhibit high thermal stabilities (Figure S2, Supporting Information). A sharp weight loss occurs in the temperature range 360–470 °C for **1** (74.8%) and 380–480 °C for **2** (72.7%), corresponding to the removal of ligands and decomposition of the framework. The final residues of complexes **1** and **2** were found to be amorphous and could not be identified.

Magnetic Properties

The temperature dependences of the magnetic susceptibilities of **1** and **2** under an applied field of 5000 Oe are shown in Figure 5 in the form of an $\chi_m T$ vs. T plot, where χ_m is the molar magnetic susceptibility per formula unit. At room temperature, the $\chi_m T$ value of **1** is 3.35 emu mol^{-1} K per Fe^{II} ion, corresponding to an average g value of 2.11. This is in agreement with the typical value for a high-spin Fe^{II} ion with some orbital contributions.[17] As the temperature is lowered, the $\chi_m T$ value remains almost constant in the range 300–50 K and then rapidly decreases to 1.44 emu mol^{-1} K at 2 K. The magnetic susceptibility above 2.5 K follows the Curie–Weiss equation $\chi_m = C/(T - \theta)$ with C = 3.37 emu mol^{-1} K and θ = –2.01 K. Such behaviour is consistent with a weak antiferromagnetic coupling interaction between the magnetic centres.

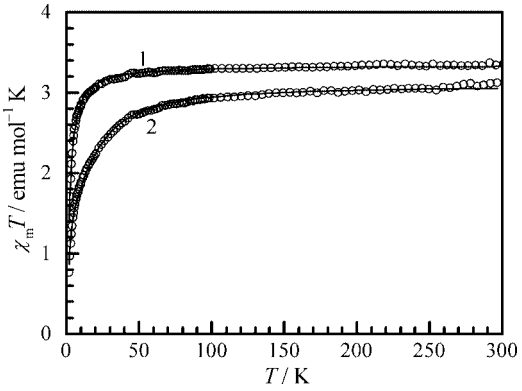

Figure 5. Temperature dependence of $\chi_m T$ for complexes **1** and **2**, the solid lines represent the best fits obtained from the models described in the text.

In the structure of **1**, the carboxylate-bridged dinuclear units are connected by 4,4′-Bpy and Tdc units to form the 3D framework. The Fe–Fe distance of 4.149 Å over the μ_2-carboxylate bridge is much shorter than those over the 4,4′-Bpy (11.49 Å) and the Tdc (10.38 Å) bridges and, consequently, the exchange coupling through the double μ_2-carboxylate bridge in the dinuclear subunits should be dominant. In order to obtain reliable simulation results, the magnetic behaviour of **1** was analysed using an analytical expression[18] based on the Hamiltonian taking into account the anisotropy g and the zero-field-splitting term in Equation (1).

$$H = g_{\perp}\beta H_{\perp}[{}^1/_2(S_1^+ + S_1^- + S_2^+ + S_2^-)] + g_{\parallel}\beta H_{\parallel}(S_{z1} + S_{z2}) - 2J[S_{z1}S_{z2} + {}^1/_2(S_1^+S_2^-) + {}^1/_2(S_1^-S_2^+)] + D(S_{z1}^2 + S_{z2}^2) \quad (1)$$

In addition, a molecular field approximation[19] was applied to Equation (1) to account for the interdimer exchange interaction (zJ') in the 3D system [Equation (2)].

$$\chi_m = \chi_{di}/(1 - 2zJ'\chi_{di}/Ng^2\beta^2) \quad (2)$$

Calculations were performed with the MAGPACK package.[20] The best fit was obtained with the following sets of parameters: J = –0.242 cm^{-1}, $g_{\parallel}$ = 2.015, $g_{\perp}$ = 2.289, D = 0.09 cm^{-1}, zJ' = 0 and an agreement factor R {defined as $R = \Sigma[(\chi_m T)_{calcd} - (\chi_m T)_{obs}]^2/\Sigma(\chi_m T)_{obs}^2$} of 4.18 × 10^{-5}. The value obtained for D is smaller and the ratio of $|J|/D$ is equal to 2.69. When J is much larger or smaller than D, exchange coupling or ZFS will be dominant and the smaller term can be treated as a perturbation. Thus, the decreases in $\chi_m T$ at lower temperatures are mainly due to antiferromagnetic coupling for complex **1**.

For **2**, the $\chi_m T$ value at room temperature is equal to 3.15 emu mol^{-1} K, which is much higher than the spin-only value of 1.875 emu mol^{-1} K expected for an isolated high spin Co^{II} ion with $S = {}^3/_2$ and g = 2.00 owing to the orbital contribution of the Co^{II} ion.[21] Upon cooling, the $\chi_m T$ value slightly decreases until around 50 K, then rapidly decreases to 0.76 emu mol^{-1} K at 2 K. Above 32 K, the

magnetic data follow the Curie–Weiss law with $C = 3.20\ \text{emu mol}^{-1}\,\text{K}$ and $\theta = -8.8$ K. The negative Weiss constant suggests an antiferromagnetic interaction between the Co^{II} ions. The presence of a small maximum in χ_m at 2.5 K is indicative of long-range antiferromagnetic ordering (Figure 6a). Complex **2** has the same structure as **1** and in order to fit the magnetic data of **2** quantitatively, we used the MAGPACK package[20] with a similar Hamiltonian model and taking into account the anisotropy g, the zero-field splitting parameter D ($S_1 = S_2 = {}^3/_2$) and the molecular field approximation[19] for the interdimer exchange interaction (zJ'). The results of the best fit of the experimental data in the whole temperature range are shown in Figure 5 with $J = -0.37\ \text{cm}^{-1}$, $g_{\parallel} = 2.42$, $g_{\perp} = 2.85$, $D = 21.00\ \text{cm}^{-1}$, $zJ' = -0.001\ \text{cm}^{-1}$ and $R = 1.25 \times 10^{-4}$. The D value is larger than the $|J|$ value and so the decreases in $\chi_m T$ at lower temperatures are mainly due to the zero-field splitting of complex **2**. Until now, only a few Co^{II} complexes bridged by carboxylate groups in a *syn-syn* mode have been rigorously studied from a magnetic point of view due to inherent difficulties resulting from strong spin-orbit coupling and magnetic anisotropy orbital degeneracy. Antiferromagnetic interactions are generally observed in these complexes.[22] The complex magnetic behaviour of Co^{II} ions did not allow us to accurately simulate the magnitude of the magnetic interaction taking into account all factors, thus the value of D obtained for **2** is larger than that for **1**.

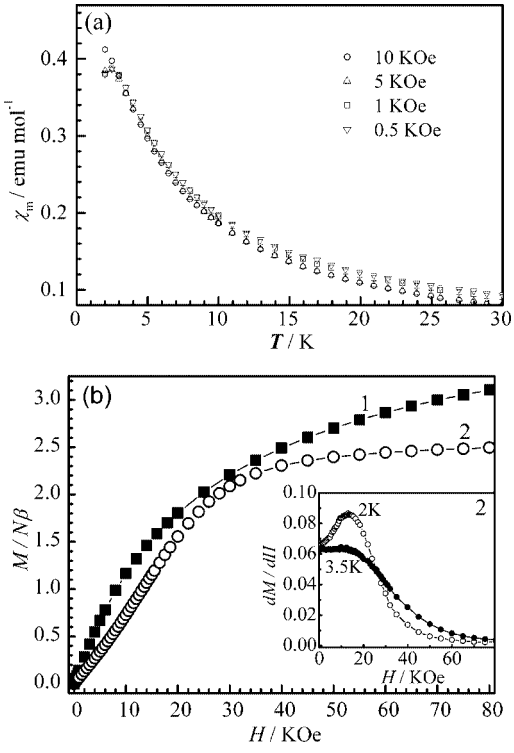

Figure 6. (a) Temperature-dependent molar magnetic susceptibilities of **2** measured at different external fields; (b) field-dependent magnetisations of **1** and **2** at 2 K. The inset shows the dM/dH derivative curves of **2** at 2 K and 3.5 K.

In fact, the Fe1–O1 (2.387 Å) and Co1–O1 (2.333 Å) bonds are much longer than the others in the equatorial planes in the structures of **1** and **2**. Ignoring these bonds, we can think of the Fe^{II} and Co^{II} centres as being in distorted trigonal-bipyramidal rather than distorted octahedral environments. The idealised trigonal-bipyramidal geometry belongs to the D_{3h} point group and the orbital momentum is quenched except for the E′ and E″ terms. However, when the structure is distorted and the symmetry deviates from pure D_{3h}, the quenching of the ground $^4A_2'$ term may not be sufficient and an admixture of the upper $^4E''$ term may bring the orbital momentum into the ground term, resulting in an obviously high μ_{eff} value and a deviation of g from 2.0.[23] In **2**, the μ_{eff} value (5.02 μ_B) is much higher than the spin-only value (3.87 μ_B) but lies in the range of 4.26–5.03 μ_B for trigonal-bipyramidal cobalt(II) complexes.[24]

In comparison with **1**, the magnetic behaviour of **2** is more complex in the low-temperature range. The small maximum of χ_m at around 2.5 K only appears at low field. When the external field is increased, this maximum vanishes above 10 kOe (Figure 6a). Furthermore, the field-dependent magnetisation of **1** exhibits a smooth increase at 2 K, reaching 3.1 $N\beta$ at 80 kOe which is less than the expected saturation value of 4 $N\beta$ for a magnetically isolated Fe^{II} centre with $g = 2.0$, while the magnetisation of **2** shows a sigmoid-like curve and gives a saturation value of 2.5 $N\beta$ at 80 kOe (Figure 6b). For the Co^{II} ion, an $S = {}^1/_2$ ground state is usually observed at low temperatures due to the overall effect of the crystal field and spin-orbit coupling. The saturation magnetisation value of **2** is within the range expected for a free cobalt ion with an effective $S = {}^1/_2$ and large anisotropic g values ranging from 4.1 to 5.0.[25]

The disappearance of the χ_m maximum at higher fields and the sigmoid-like magnetisation curve of **2** suggest the occurrence of a field-induced magnetic transition. The transition field, determined by the dM/dH derivative curve is ca. 12 kOe at 2 K (inset in Figure 6b). The AC isothermal magnetisation measurements at 2 K with the DC field from 0 to 50 kOe display a peak value of the in-phase component of the susceptibility (χ') at 11 kOe, consistent with the transition observed in the dM/dH curve. It is worthy of note that a nonzero out-of-phase component of the AC susceptibility (χ'') appears at 17 kOe with a further increase in the applied field, indicating the occurrence of the second magnetic transition. Additional measurements at 3.5 and 5 K show the temperature dependence of the second magnetic transition, the H value increases slightly as the temperature increases (Figure 7).

The magnetic behaviour of **2** is analogous to some observations in the complexes with field-induced spin-flop phase transitions (SF), which is characteristic for antiferromagnetic (AF) systems with weak anisotropy.[26] Although this transition does not generally appear in a system with large anisotropy such as the Ising mode, similar transition behaviour has been discussed for several Co^{II} complexes.[27] In **2**, the spin-flop field (H_{SF}) appears at 11 kOe, corresponding to a transition from an antiferromagnetic to a spin-flop state. The AF-SF transition is a first-order transition and there is a discontinuity in the magnetisation on crossing the

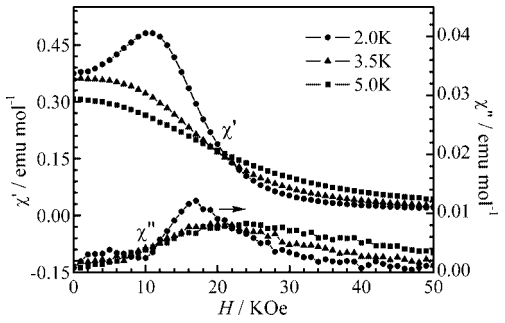

Figure 7. Field-dependent AC magnetic susceptibilities of **2** measured at different temperatures.

AF-SF phase boundary. Thus, an inflexion can be observed in the $M(H)$ curve and a peak also appears in the $\chi'(H)$ plot.[26] Another critical field (H_C) is not evident in $\chi'(H)$ although an obvious peak around 17 kOe can be observed in the $\chi''(H)$ curve, which can be identified as the second-order transition field (H_C) from a spin-flop to a ferromagnetic-like state.[28,29] The lack of a sharp conversion in $\chi'(H)$ suggests that this second phase-transition process is rather gradual.[29] To further substantiate the spin-flop transition in **2**, additional temperature-dependent AC magnetic susceptibility measurements at different DC fields were carried out (Figure 8). The zero-field AC magnetic susceptibility measurements exhibit a maximum value of χ' at 2.5 K and a negligible χ'' value, in agreement with the existence of antiferromagnetic ordering. The data measured at 12 kOe clearly show the disappearance of the χ' maximum, indicating that an antiferromagnetic coupling has been overcome. At an applied field of 17 kOe, χ' exhibits a new broad peak around 6.9 K, accompanied by a maximum peak of χ'' at somewhat lower temperatures. This feature is quite consistent with a ferromagnetic-like state. It is also notable that the similar small peaks around 6.9 K already appear in $\chi'(T)$ and $\chi''(T)$ plots at 12 kOe, which is in accordance with the continuity and gradualness of this second-order phase transition. With the above results, the anisotropy field $H_A \approx 0.71$ kOe and the exchange field $H_E \approx 1.21$ kOe were estimated based on the mean-field relation $H_{SF} = (2H_EH_A - H_A^2)^{1/2}$ and $H_C = 2H_E - H_A$.[30] The anisotropy constant $a = H_A/H_E$ is 0.59. Although no related parameter can be found in Co^{II} complexes for comparison, a lower anisotropy field in **2** suggests that its magnetisation process can possibly proceed through the spin-flop-like transition.[31]

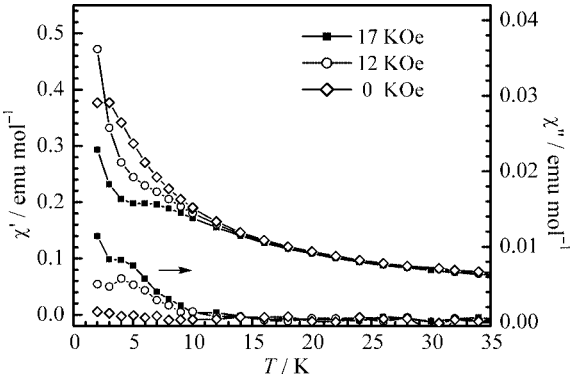

Figure 8. Temperature dependence of the AC magnetic susceptibilities of **2** measured in a field amplitude of 3 Oe (711 Hz) and a DC bias field of 0, 12 and 17 kOe.

Conclusions

In summary, two novel 3D porous frameworks were hydrothermally synthesised and structurally characterised. Metal ions are connected by chelating and bridging carboxylate groups of Tdc groups to form 2D rectangle-grid layers containing dinuclear subunits in an approximately perpendicular orientation. The interconnection of the 2D layers by the secondary metal linker (4,4′-Bpy) leads to the doubly pillared-layered 3D architecture with twofold interpenetration. Variable-temperature magnetic susceptibility measurements reveal weak antiferromagnetic coupling interactions in both complexes and a field-induced magnetic transition can be observed in **2**.

Experimental Section

General: All the syntheses were performed in Parr Teflon-lined stainless steel autoclaves under autogenous pressure. All chemicals were analytical reagent grade and were used as received. IR spectra were recorded with a Spectrum One FT-IR spectrophotometer in KBr pellets in the range 4000–400 cm^{-1}. Elemental analyses were determined with an Elementar Vario EL III elemental analyser. The thermal analysis was performed under air with a Netzsch STA449C thermal analyser at a heating rate of 20 °C min^{-1}. Magnetic susceptibilities were measured using a Quantum Design PPMS-9T system. Diamagnetic corrections were estimated from Pascal's constants. The pore-volume analysis was performed with the PLATON software package.

Synthesis of $[Fe^{II}(tdc)(bpy)]_n$ (1): This compound was synthesised by the hydrothermal method. A mixture of $FeCl_3·6H_2O$ (65 mg, 0.24 mmol), H_2Tdc (70 mg, 0.41 mmol), NaOH (33 mg, 0.83 mmol) and 4,4′-Bpy (74 mg, 0.47 mmol) in H_2O (5 mL) was homogenised at room temperature for 20 min. The resultant mixture was transferred and sealed in a Teflon-lined steel autoclave (23 mL) at 120 °C for 3 d and was then cooled to room temperature at a rate of 1.7 K h^{-1}. The dark-red crystals were isolated in 35.9% yield based on Fe. $C_{16}H_{10}FeN_2O_4S$ (382.17): calcd. C 50.28, H 2.64, N 7.33; found C 49.82, H 2.98, N 7.36. IR (KBr): $\tilde{\nu}$ = 3434 (m), 1604 (s), 1570 (s), 1524 (m), 1490 (w), 1414 (s), 1384 (vs), 1221 (w), 1072 (w), 1046 (w), 1033 (w), 1008 (w), 818 (m), 769 (m), 731 (w), 684 (w), 631 (m), 475 (m) cm^{-1}.

Synthesis of $[Co^{II}(tdc)(bpy)]_n$ (2): This compound was obtained using a procedure similar to that of **1**, except that $CoCl_2·6H_2O$ was used instead of $FeCl_3·6H_2O$. The pink crystals were isolated in 27.6% yield based on Co. $C_{16}H_{10}CoN_2O_4S$ (385.25): calcd. C 49.88, H 2.62, N 7.27; found C 49.56, H 3.04, N 7.54. IR (KBr): $\tilde{\nu}$ = 3435 (m), 1607 (s),1564 (s),1524 (m),1491 (w),1416 (s),1385 (vs),1221 (w), 1075 (w), 1045 (w), 1029 (w), 1011 (w), 821 (m), 767 (m), 732 (w), 682 (w), 634 (m), 477 (m) cm^{-1}.

X-ray Crystallographic Study: The intensity data of **1** were collected with a Rigaku CCD diffractometer with graphite-monochromated Mo-K_α radiation (λ = 0.71073 Å) at room temperature. An empiri-

Table 1. Crystallographic data for complexes **1** and **2**.

	1	**2**
Empirical formula	$C_{16}H_{10}FeN_2O_4S$	$C_{16}H_{10}CoN_2O_4S$
Formula mass	382.17	385.25
Crystal system	orthorhombic	orthorhombic
Space group	*Pccn*	*Pccn*
a [Å]	18.2626(13)	17.9459(5)
b [Å]	11.4913(9)	11.4012(3)
c [Å]	16.0515(10)	16.2390(5)
V [Å^3]	3368.6(4)	3322.58(16)
Z	8	8
$D_{calcd.}$ [g cm^{-3}]	1.507	1.540
F(000)	1640	1560
Crystal size [mm]	0.30 × 0.10 × 0.03	0.45 × 0.18 × 0.10
Range for data collection [°]	3.10–27.48	2.12–25.66
Reflections collected	24699	16819
Independent reflections	3858	3140
Number of parameters	217	217
Refinement method	full-matrix least squares on F^2	full-matrix least squares on F^2
Goodness-of-fit on F^2	1.029	1.001
R_1 [$I > 2\sigma(I)$]	0.0713	0.0656
wR_2 (all data)	0.1410	0.1295

cal absorption correction for **1** was performed using the CrystalClear program.[32] The crystal structure determination of **2** was performed with a Siemens SMART CCD diffractometer with graphite-monochromated Mo-K_α radiation (λ = 0.71073 Å) at room temperature. An empirical absorption correction for **2** was applied using the SADABS program.[33] The structure was solved by direct methods and refined by full-matrix least-squares fitting on F^2 using the SHELXS-97[34] and SHELXL-97[35] programs. All non-hydrogen atoms were refined with anisotropic thermal parameters. Hydrogen atoms were located by geometric calculations. Crystallographic data and structural refinements for **1** and **2** are summarised in Table 1. Selected bond lengths and angles for **1** and **2** are listed in Table 2. CCDC-298904 (**1**) and -298903 (**2**) contain the supplementary crystallographic data for this paper. These data can be obtained free of charge from The Cambridge Crystallographic Data Centre via www.ccdc.cam.ac.uk/data_request/cif.

Table 2. Selected bond lengths [Å] and angles [°] for **1** and **2**.

Complex **1**			
Fe1–O1	2.387(3)	Fe1–O4B^{i}	1.999(3)
Fe1–O2	2.116(3)	Fe1–N2D^{iii}	2.195(3)
Fe1–N1	2.198(3)	Fe1–O3A^{ii}	2.090(3)
O1–Fe1–O2	58.07(10)	O1–Fe1–N1	92.09(12)
O2–Fe1–N2D^{iii}	91.30(13)	O2–Fe1–N1	90.25(13)
O3A^{ii}–Fe1–O2	91.29(11)	O3A^{ii}–Fe1–N2D^{iii}	91.27(12)
O3A^{ii}–Fe1–N1	90.37(12)	O3A^{ii}–Fe1–O2	91.29(11)
O4B^{i}–Fe1–N1	87.64(14)	O4B^{i}–Fe1–O3A^{ii}	117.90(12)
O4B^{i}–Fe1–O1	92.82(12)	O4B^{i}–Fe1–O1	92.82(12)
O4B^{i}–Fe1–N2D^{iii}	90.19(14)	N2D^{iii}–Fe1–N1	177.71(13)
N2D^{iii}–Fe1–O1	87.31(12)		
Complex **2**			
Co1–O1	2.333(4)	Co1–O4B^{i}	1.999(3)
Co1–O2	2.110(4)	Co1–N2D^{iii}	2.141(4)
Co1–N1	2.154(4)	Co1–O3A^{ii}	2.050(3)
O1–Co1–O2	59.03(13)	O1–Co1–N1	92.75(16)
O1–Co1–N2D^{iii}	85.75(16)	O2–Co1–N1	88.73(16)
O3A^{ii}–Co1–O1	152.45(14)	O3A^{ii}–Co1–N2D^{iii}	91.88(16)
O3A^{ii}–Co1–N1	90.21(16)	O3A^{ii}–Co1–O2	93.69(14)
O4B^{i}–Co1–N1	85.99(17)	O4B^{i}–Co1–O3A^{ii}	113.67(15)
O4B^{i}–Co1–O2	152.11(15)	O4B^{i}–Co1–O1	93.87(14)
O4B^{i}–Co1–N2D^{iii}	92.44(17)	N2D^{iii}–Co1–N1	177.76(17)
N2D^{iii}–Co1–O2	91.93(17)		

(i) 1.5 – *x*, *y*, –0.5 + *z*; (ii) –0.5 + *x*, 1 – *y*, 0.5 – *z*; (iii) *x*, –1 + *y*, *z*

Supporting Information (see footnote on the first page of this article): Additional two plots including IR spectrum and TGA curve (Figures S1 and S2).

Acknowledgments

The authors acknowledge the financial support of the Natural Science Foundation of China (No. 50372069/20201010), the Natural Science Foundation of Fujian Province of China (No. E0220003) and the Ministry of Education/Personnel of China.

[1] O. M. Yaghi, H. Li, C. Davis, D. Richardardson, T. L. Groy, *Acc. Chem. Res.* **1998**, *31*, 474–484.
[2] D. L. Long, R. J. Hill, A. J. Blake, N. R. Champness, P. Hubberstey, C. Wilson, M. Schröder, *Chem. Eur. J.* **2005**, *11*, 1384–1391.
[3] L. Pan, D. H. Olson, L. R. Ciemnolonski, R. Heddy, J. Li, *Angew. Chem. Int. Ed.* **2006**, *45*, 616–619.
[4] E. Coronado, J. R. Galán-Mascarós, C. J. Gómez-Garcia, V. Laukhin, *Nature* **2000**, *408*, 447–449.
[5] P. G. Lacroix, I. Malfant, S. Benard, P. Yu, E. Riviere, K. Nakatani, *Chem. Mater.* **2001**, *13*, 441–449.
[6] S. Karasawa, Y. Sano, T. Akita, N. Koga, T. Itoh, H. Iwamura, P. Rabu, M. Drilion, *J. Am. Chem. Soc.* **1998**, *120*, 10080–10087.
[7] B.-B. Ding, Y.-Q. Weng, Z.-W. Mao, C.-K. Lam, X.-M. Chen, B.-H. Ye, *Inorg. Chem.* **2005**, *44*, 8836–8845.
[8] T. K. Maji, K. Uemura, H. Chang, R. Matsuda, S. Kitagawa, *Angew. Chem. Int. Ed.* **2004**, *43*, 3269–3272.
[9] B.-Q. Ma, P. Coppens, *Chem. Commun.* **2003**, 412–413.
[10] M. Kondo, T. Okubo, A. Asami, S.-i. Noro, T. Yoshitomi, S. Kitagawa, T. Ishii, H. Matsuzaka, K. Seki, *Angew. Chem. Int. Ed.* **1999**, *38*, 140–143.
[11] X.-L. Wang, C. Qin, E.-B. Wang, Y.-G. Li, C.-W. Hu, L. Xu, *Chem. Commun.* **2004**, 378–379.
[12] H. Chun, D. N. Dybtsev, H. Kim, K. Kim, *Chem. Eur. J.* **2005**, *11*, 3521–3529.
[13] T. K. Maji, M. Ohba, S. Kitagawa, *Inorg. Chem.* **2005**, *44*, 9225–9231.
[14] B.-L. Chen, K.-F. Mok, S.-C. Ng, M. G. B. Drew, *New J. Chem.* **1999**, *23*, 877–883. A further search in the CCDC data-

base (version 1.8) does not show this kind of coordination mode.
[15] O. M. Yaghi, H. Li, *J. Am. Chem. Soc.* **1995**, *117*, 10401–10402.
[16] a) C.-B. Ma, C.-N. Chen, Q.-T. Liu, F. Chen, D.-Z. Liao, L.-C. Li, L.-C. Sun, *Eur. J. Inorg. Chem.* **2003**, 2872–2879 (containing orthogonal dimer); b) R.-Q. Zou, X.-H. Bu, R.-H. Zhang, *Inorg. Chem.* **2004**, *43*, 5382–5386; c) D.-P. Cheng, M. A. Khan, R. P. Houser, *Inorg. Chem.* **2001**, *40*, 6858–6859; d) J. Tao, M.-L. Tong, X.-M. Chen, *J. Chem. Soc., Dalton Trans.* **2000**, 3669–3674.
[17] a) F. E. Mabbs, D. J. Machin, *Magnetism and Transition Metals Complexes*, Chapman and Hall Ltd., London, **1973**; b) R. L. Carlin, *Magnetochemistry*, Springer-Verlag, Berlin, Heidelberg, **1986**.
[18] P. Garge, R. Chikate, S. Padhye, J.-M. Savariault, P. de Loth, J.-P. Tuchagues, *Inorg. Chem.* **1990**, *29*, 3315–3320.
[19] B. E. Myers, L. Berger, S. A. Friedberg, *J. Appl. Phys.* **1968**, *40*, 1149–1151.
[20] a) J. J. Borrás-Almenar, J. M. Clemente-Juan, E. Coronado, B. S. Tsukerblat, *Inorg. Chem.* **1999**, *38*, 6081–6088; b) J. J. Borrás-Almenar, J. M. Clemente-Juan, E. Coronado, B. S. Tsukerblat, *J. Comput. Chem.* **2001**, *22*, 985–991.
[21] M. J. Hossain, M. Yamasaki, M. Mikuriya, A. Kuribayashi, H. Sakiyama, *Inorg. Chem.* **2002**, *41*, 4058–4062.
[22] a) S. Konar, E. Zangrando, M. G. B. Drew, J. Ribas, N. R. Chaudhuri, *Dalton Trans.* **2004**, 260–266; b) D. Ghoshal, G. Mostafa, T. K. Maji, E. Zangrando, T.-H. Lu, J. Ribas, N. R. Chaudhuri, *New J. Chem.* **2004**, *28*, 1204–1213.
[23] a) Md. J. Hossain, H. Sakiyama, *Inorg. Chim. Acta* **2002**, *338*, 255–259; b) S.-Q. Bai, E.-Q. Gao, Z. He, C.-J. Fang, C.-H. Yan, *New J. Chem.* **2005**, *29*, 935–941.
[24] A. K. Patra, M. Ray, R. Mukherjee, *J. Chem. Soc., Dalton Trans.* **1999**, 2461–2466.
[25] a) W. K. Robinson, S. A. Friedberg, *Phys. Rev.* **1960**, *117*, 402–408; b) M. Drillon, E. Coronado, M. Belaiche, R. L. Carlin, *J. Appl. Phys.* **1988**, *63*, 3551–3553.
[26] R. L. Carlin, A. J. Van Duyneveldt, *Acc. Chem. Res.* **1980**, *13*, 231–236.
[27] a) P. Rabu, P. Janvier, B. Bujoli, *J. Mater. Chem.* **1999**, *9*, 1323–1326; b) X.-Y. Wang, H.-Y, Wei, Z.-M. Wang, Z.-D. Chen, S. Gao, *Inorg. Chem.* **2005**, *44*, 572–583.
[28] J. L. Manson, Q.-Z. Huang, J. W. Lynn, H.-J. Koo, M.-H. Whangbo, R. Bateman, T. Otsuka, N. Wada, D. N. Argyriou, J. S. Miller, *J. Am. Chem. Soc.* **2001**, *123*, 162–172.
[29] Y. S. You, J. H. Yoon, H. C. Kim, C. S. Hong, *Chem. Commun.* **2005**, 4116–4118.
[30] J. L. Manson, C. R. Kmety, F. Palacio, A. J. Epstein, J. S. Miller, *Chem. Mater.* **2001**, *13*, 1068–1073.
[31] P. Przychodzeń, K. Lewiński, M. Balanda, R. Pelka, M. Rams, T. Wasiutyński, C. Guyard-Duhayon, B. Sieklucka, *Inorg. Chem.* **2004**, *43*, 2967–2974.
[32] Molecular Structure Corporation & Rigaku, *CrystalClear*, version 1.36, MSC, 9009 New Trails Drive, The Woodland, TX 77381-5209, USA, and Rigaku Corporation, 3-9-12 Akishima, Tokyo, Japan, **2000**.
[33] G. M. Sheldrick, *SADABS, Program for Empirical Absorption Correction of Area Dectector Data*, University of Göttingen, Göttingen, Germany, **1996**.
[34] G. M. Sheldrick, *SHELXS-97, Program for the Solution of Crystal Structure*, University of Göttingen, Germany, **1990**.
[35] G. M. Sheldrick, *SHELXL-97, Program for the Refinement of Crystal Structure*, University of Göttingen, Germany, **1997**.

Received: May 12, 2006
Published Online: September 18, 2006

